Cascade of Kinetic Energy in Three-Dimensional Compressible Turbulence

Jianchun Wang, Yantao Yang, Yipeng Shi,* Zuoli Xiao, X. T. He, and Shiyi Chen†

State Key Laboratory for Turbulence and Complex Systems, Center for Applied Physics and Technology, Key Laboratory of High Energy Density Physics Simulation, College of Engineering, Peking University, Beijing 100871, China

(Received 26 January 2013; published 21 May 2013)

The conservative cascade of kinetic energy is established using both Fourier analysis and a new exact physical-space flux relation in a simulated compressible turbulence. The subgrid scale (SGS) kinetic energy flux of the compressive mode is found to be significantly larger than that of the solenoidal mode in the inertial range, which is the main physical origin for the occurrence of Kolmogorov's $-5/3$ scaling of the energy spectrum in compressible turbulence. The perfect antiparallel alignment between the large-scale strain and the SGS stress leads to highly efficient kinetic energy transfer in shock regions, which is a distinctive feature of shock structures in comparison with vortex structures. The rescaled probability distribution functions of SGS kinetic energy flux collapse in the inertial range, indicating a statistical self-similarity of kinetic energy cascades.

DOI: 10.1103/PhysRevLett.110.214505 PACS numbers: 47.27.E−, 47.40.−x, 47.53.+n

Compressible turbulence is of fundamental importance in a wide range of engineering flows and natural phenomena including high-temperature reactive flows, hypersonic aircrafts, and star formation in galaxies [1,2]. However, the basic processes occurring in compressible turbulence are less understood as compared to those occurring in incompressible turbulence. It is crucial to clarify the underlying physics of the interscale transfer of kinetic energy in compressible turbulence. In this Letter, we describe an investigation of Kolmogorov's $-5/3$ scaling of the kinetic energy spectrum and the conservative cascade of kinetic energy in the presence of large-scale shock waves in compressible turbulence, with a specific focus on the drastic enhancement in kinetic energy flux through shock structures.

Fully developed three-dimensional (3D) incompressible turbulence exhibits Kolmogorov's $-5/3$ energy spectrum in the inertial range that is generated and maintained by a nonequilibrium process, viz., the conservative cascade of kinetic energy from large scales to small scales [3,4]. In compressible turbulence, there are nonlinear interactions between solenoidal and compressive modes of velocity fluctuations. Moreover, quasi-2D shock waves add a new type of flow structures in addition to quasi-1D intense vortices as in incompressible turbulence, which further complicates the kinetic energy transfer process in compressible turbulence. Interestingly, the Kolmogorov's $-5/3$ energy spectrum of velocity has been reported in supersonic motions of interstellar media [5–7]. High resolution numerical simulations for supersonic isothermal turbulence showed the $-5/3$ spectrum of the density-weighted velocity $\mathbf{v} = \rho^{1/3}\mathbf{u}$, where ρ is the density and $\mathbf{u}$ is the velocity [8,9]. Aluie [10,11] proved that the kinetic energy cascades conservatively in compressible turbulence, provided that the pressure-dilatation cospectrum decays at a sufficiently rapid rate. This analysis was further supported by numerical simulations of both forced and decaying compressible turbulence [12].

Here, we utilize a novel hybrid numerical method [13] to simulate a compressible turbulence in a cubic box at a 1024^3 grid resolution. We apply large-scale force to both solenoidal and compressive components of the velocity field [14–16]. The flow is evolved to about $6T_e$, where the large-eddy turn over time $T_e = \sqrt{3}L/u^{\mathrm{rms}}$, where L is the integral length scale and u^{rms} is the rms velocity magnitude. Various statistics of the simulated flow are averaged over the time interval $3.6 < t/T_e < 6.0$. The turbulent Mach number $M_t = u^{\mathrm{rms}}/\langle c\rangle = 0.62$, where $\langle c\rangle$ is the average sound speed, and the Taylor microscale Reynolds number $R_\lambda = 160$. The highest local Mach number exceeds 2.5, and sheetlike shock waves of large-scale size are generated in the simulated flow.

Helmholtz decomposition of the density weighted velocity $\mathbf{w} = \sqrt{\rho}\mathbf{u}$ yields a solenoidal component $\mathbf{w}^s$ and a compressive component $\mathbf{w}^c$: $\mathbf{w} = \mathbf{w}^s + \mathbf{w}^c$, where $\nabla \cdot \mathbf{w}^s = 0$ and $\nabla \times \mathbf{w}^c = 0$. The average kinetic energy $E_k = \langle w^2/2\rangle$ can be decomposed by $E_k = E_k^s + E_k^c$, where $E_k^s = \langle (w^s)^2/2\rangle$ and $E_k^c = \langle (w^c)^2/2\rangle$. In our simulation, $E_k^c/E_k^s = 2.7$; i.e., the compressive kinetic energy is significantly larger than its solenoidal counterpart. Figure 1(a) shows that the kinetic energy spectrum exhibits a $-5/3$ scaling and its compressive component displays a -2 scaling in the inertial range of $4 \le k \le 20$ (see Supplemental Material [17]). To clarify the k^{-2} compressive spectrum, we consider the equation of the velocity potential Ψ defined by $\mathbf{u}^c = -\nabla\Psi$ (where $\mathbf{u}^c$ is the compressive velocity component, see Supplemental Material [17]):

$$\partial_t \Psi - \frac{1}{2}\nabla\Psi \cdot \nabla\Psi = \frac{4\nu}{3}\nabla^2\Psi + N_p + N_{\mathrm{sol}} + F, \quad (1)$$

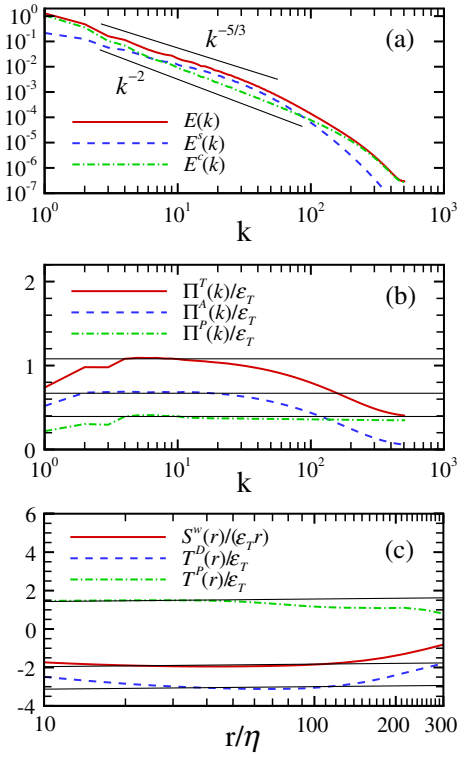

FIG. 1 (color online). (a) Spectra for kinetic energy and its two components; (b) Fourier-space kinetic energy flux; (c) structure functions in the physical-space kinetic energy flux.

where, $N_p = \nabla^{-2}[\nabla \cdot (\nabla p/\rho)]$ and p is the pressure. $N_{\rm sol}$ represents the impact of the solenoidal velocity component. ν is the coefficient of viscosity, and F is the potential of external force. According to the theory of 3D Burgers turbulence [18], large-scale shock waves can be generated through the effect of potential gradient square $\nabla\Psi \cdot \nabla\Psi$, leading to a k^{-2} spectrum of $\mathbf{u}^c$ at moderate and high Mach numbers. Moreover, we find that the two spectra for $\mathbf{u}^c$ and $\mathbf{w}^c$ are almost identical, indicating the negligible effect of density in our simulated flow.

In Fig. 1(b), we present the kinetic energy flux due to the advection and the pressure, namely,

$$\Pi^T(k) = \Pi^A(k) + \Pi^P(k), \tag{2}$$

where $\Pi^A(k) = \sum_{|\mathbf{k}|<k}\langle \mathrm{Re}[\hat{\mathbf{w}}^*(\mathbf{k}) \cdot (\widehat{\mathbf{u}\cdot\nabla\mathbf{w}} + \widehat{\mathbf{w}\theta}/2)(\mathbf{k})]\rangle$ and $\Pi^P(k) = \sum_{|\mathbf{k}|<k}\langle \mathrm{Re}[\hat{\mathbf{w}}^*(\mathbf{k}) \cdot (\widehat{\nabla p/\sqrt{\rho}})(\mathbf{k})]\rangle$ [19,20]. The energy flux has been normalized by the total dissipation $\epsilon_T = -\langle p\theta\rangle + \epsilon_0$ [21], i.e., the total conversion rate of kinetic energy into internal energy by the pressure-dilatation work $-\langle p\theta\rangle$ and the viscous dissipation ϵ_0. The kinetic energy flux is approximately constant in the inertial range of $4 \le k \le 20$. Particularly, the ratio of $\Pi^A(k)$ to $\Pi^P(k)$ is about 0.65:0.35 in the inertial range, indicating the remarkable effect of pressure on the kinetic energy transfer.

We now introduce the physical-space kinetic energy flux defined by [3,22]

$$\epsilon(\mathbf{r}) \equiv -\partial_t\langle \mathbf{w}(\mathbf{x})\mathbf{w}(\mathbf{x}+\mathbf{r})/2\rangle|_{\rm NL}, \tag{3}$$

where, $\partial_t()|_{\rm NL}$ denotes the time-rate-of-change by the nonlinear terms including advection and pressure. Specifically, the flux for homogeneous isotropic turbulence (see Supplemental Material [17]) is $\epsilon(\mathbf{r}) = [-\nabla_{\mathbf{r}}\cdot(S^w(r)\mathbf{r}/r) + T^D(r) + T^P(r)]/4$, where $S^w(r) = \langle(\delta\mathbf{w})^2\delta\mathbf{u}\cdot\mathbf{r}/r\rangle$ is a third-order structure function of velocity. $T^D(\mathbf{r}) = \langle\delta\mathbf{w}\cdot(\theta\mathbf{w}' - \theta'\mathbf{w})\rangle$ and $T^P(\mathbf{r}) = 2\langle\mathbf{w}'\cdot(\nabla p/\sqrt{\rho}) + \mathbf{w}\cdot(\nabla' p'/\sqrt{\rho'})\rangle$, respectively, represent the impact of dilatational motion and pressure. Here, increments of $\mathbf{w}$ and $\mathbf{u}$ are defined by $\delta\mathbf{w} = \mathbf{w}' - \mathbf{w}$ and $\delta\mathbf{u} = \mathbf{u}' - \mathbf{u}$, respectively, and the prime is used to denote variables at the point $\mathbf{x}' = \mathbf{x} + \mathbf{r}$. We plot the rescaled third-order structure function $S^w(r)/r$ as a function of the separation r in Fig. 1(c). The separation r has been normalized by the Kolmogorov length scale η. The function $S^w(r)/r$ is nearly constant in an inertial range, such that $S^w \approx -C_0^w\epsilon_T r$, similar to the case of incompressible turbulence, but the coefficient $C_0^w = 1.95$ is substantially larger than $C_0 = 4/3$ found in incompressible turbulence [23]. Moreover, Fig. 1(c) shows that $T^D(r)/\epsilon_T \approx -C_0^D$ and $T^P(r)/\epsilon_T \approx C_0^P$ in the inertial range, where $C_0^D = 3.15$ and $C_0^P = 1.45$. Consequently, the physical-space kinetic energy flux via advection [i.e., the first and second terms in $\epsilon(\mathbf{r})$] is about $0.68\epsilon_T$, and that via pressure is about $0.36\epsilon_T$.

We suppose that the dissipation acts mainly at the smallest scales of turbulence [10,11], leading to $\epsilon(\mathbf{r}) = \epsilon_T$ for the separation $\mathbf{r}$ in the inertial range in compressible turbulence driven by a proper large-scale force. This yields a new flux relation in compressible isotropic turbulence [22–24], which can be expressed by

$$\nabla_{\mathbf{r}}\cdot\left(S^w(r)\frac{\mathbf{r}}{r}\right) = -4\epsilon_T + T^D(r) + T^P(r). \tag{4}$$

Particularly, $C_0^w = (4 + C_0^D - C_0^P)/3$ in the inertial range, in good agreement with the numerical results. The effect of dilatation is to enlarge the coefficient C_0^w, while the effect of pressure is to decrease C_0^w. We note that the impact of external forcing is small, considering that the variation in the density field is not very strong in our simulated flow compared to that in the supersonic isothermal turbulence at the turbulent root-mean-square Mach number 6 [24]. In the limit of incompressible turbulence, this relation reduces to

$$\nabla_{\mathbf{r}}\cdot\langle(\delta\mathbf{u})^2\delta\mathbf{u}\rangle = -4\epsilon_0, \tag{5}$$

which is equivalent to Kolmogorov's 4/5 law in isotropic incompressible turbulence [23].

We now employ a "coarse-graining" approach [10] to study the cascade of kinetic energy. We begin with the definition of a classically filtered field $\bar{\mathbf{a}}(\mathbf{x}) \equiv \int d^3\mathbf{r} G_l(\mathbf{r})\mathbf{a}(\mathbf{x}+\mathbf{r})$, where $G_l(\mathbf{r}) \equiv l^{-3}G(\mathbf{r}/l)$ is the kernel and $G(\mathbf{r})$ is a normalized window function. The Favre filtered field is defined as $\tilde{\mathbf{a}} \equiv \overline{\rho\mathbf{a}}/\bar{\rho}$. The filtered equation for the kinetic energy reads

$$\partial_t \frac{\bar{\rho}|\tilde{\mathbf{u}}|^2}{2} + \nabla \cdot \mathbf{J}_l = -\Pi_l - \Lambda_l - \Phi_l - D_l + \varepsilon^{\mathrm{inj}}, \quad (6)$$

where, the kinetic energy flux due to the subgrid scale (SGS) stress is $\Pi_l = -\nabla\tilde{\mathbf{u}}:[\bar{\rho}(\widetilde{\mathbf{u}\mathbf{u}} - \tilde{\mathbf{u}}\tilde{\mathbf{u}})]$, the energy flux due to the turbulent mass flux $\Lambda_l = \nabla\bar{p}\cdot(\overline{\rho\mathbf{u}} - \bar{\rho}\,\tilde{\mathbf{u}})/\bar{\rho}$, and the large scale pressure-dilatation $\Phi_l = -\bar{p}\theta_l$ [10]. $\mathbf{J}_l$ is the spatial transport flux of large-scale kinetic energy, D_l the viscous dissipation term, and $\varepsilon^{\mathrm{inj}}$ the energy injected by forcing. We present the spatial average of the SGS energy flux and the pressure-dilatation in Fig. 2(a). The filter width l has been normalized by the Kolmogorov length scale η. The pressure-dilatation Φ_l is nearly constant at scales $l/\eta < 100$, qualitatively consistent with the result reported by Aluie *et al.* [12]. The average of both Π_l and Λ_l are nearly constant over an inertial range $20 < l/\eta < 100$, indicating the existence of a conservative cascade of kinetic energy through the inertial range [10–12].

Helmholtz decomposition on the SGS energy flux yields $\Pi_l = \Pi_l^s + \Pi_l^c$, where $\Pi_l^s = -\nabla(\tilde{\mathbf{w}}^s/\sqrt{\bar{\rho}}):[\bar{\rho}(\widetilde{\mathbf{u}\mathbf{u}} - \tilde{\mathbf{u}}\tilde{\mathbf{u}})]$ and $\Pi_l^c = -\nabla(\tilde{\mathbf{w}}^c/\sqrt{\bar{\rho}}):[\bar{\rho}(\widetilde{\mathbf{u}\mathbf{u}} - \tilde{\mathbf{u}}\tilde{\mathbf{u}})]$, that is, the turbulent stress acting against the large-scale strain which is due to the solenoidal or compressive component of the density-weighted velocity, where $\tilde{\mathbf{w}}^s$ and $\tilde{\mathbf{w}}^c$ are, respectively, the solenoidal and compressive components of $\tilde{\mathbf{w}} = \sqrt{\bar{\rho}}\tilde{\mathbf{u}}$. We note that the average of Π_l^s (Π_l^c) is exactly equal to the average flux of $\tilde{E}^s$ (or $\tilde{E}^c$) from large scales to subgrid scales, owing to SGS stress, where $\tilde{E}^s = \langle(\tilde{w}^s)^2/2\rangle$ and $\tilde{E}^c = \langle(\tilde{w}^c)^2/2\rangle$. Figure 2(b) shows that the average SGS energy flux of both solenoidal and compressive modes is nearly constant in the inertial interval, namely, $\langle\Pi_l^s\rangle \approx 0.075\epsilon_T$ and $\langle\Pi_l^c\rangle \approx 0.62\epsilon_T$. Thus, the compressive component of the kinetic energy cascade is significantly faster than its solenoidal counterpart, leading to the dominance of the solenoidal kinetic energy spectrum at high wave numbers in the inertial range. Therefore, both the overall kinetic energy spectrum and its solenoidal component exhibit Kolmogorov's $-5/3$ scaling at high wave numbers in the inertial range. This is further confirmed by numerical simulation of Euler equations with an eighth-order hyperviscosity [13], at the same turbulent Mach number $M_t = 0.62$ and 512^3 grid resolution [see Fig. 2(c)]. The power-law exponents are found to be -1.66 and -2.02, respectively for the solenoidal and compressive kinetic energy spectra in the range of $4 \le k \le 30$ by least square estimation (see Supplemental Material [17]). Since the inertial-range statistics are independent of the dissipation mechanism [25,26], both the overall kinetic energy spectrum and its solenoidal component should have a clear $-5/3$ scaling at higher Reynolds numbers in compressible turbulence with normal viscosity.

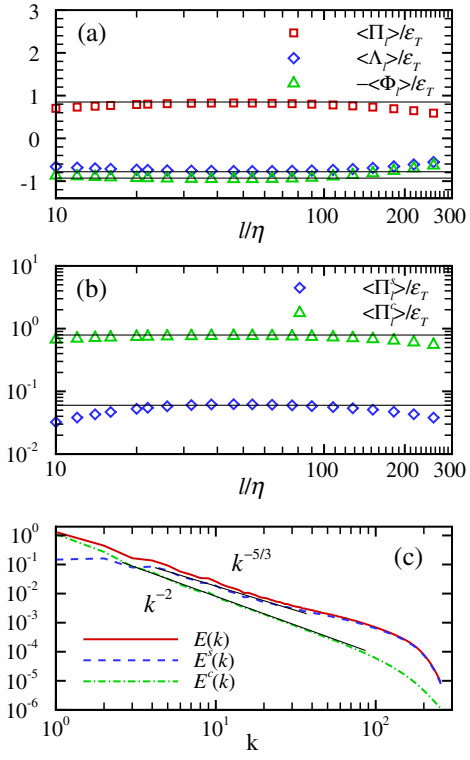

FIG. 2 (color online). (a) SGS kinetic energy flux and large scale pressure-dilatation work; (b) solenoidal and compressive components of SGS kinetic energy flux Π_l; (c) spectra for kinetic energy and its two components in the hyperviscosity simulation.

Figure 3 shows a 3D visualization for the isosurfaces of the solenoidal component Π_l^s and the compressive component Π_l^c of kinetic energy flux. Only the 512^3 mesh points are shown. $(\Pi_l^s)^{\mathrm{rms}}$ and $(\Pi_l^c)^{\mathrm{rms}}$ are the rms values of Π_l^s and Π_l^c, respectively. The figure reveals a dramatic difference between the spatial structures of Π_l^s and Π_l^c. The isosurfaces of Π_l^c have large-scale sheetlike structures, whereas the isosurfaces of Π_l^s tend to exhibit coarse-grained blocklike structures that are similar to those in incompressible turbulence [27]. This observation indicates a significantly greater intermittency of the compressive

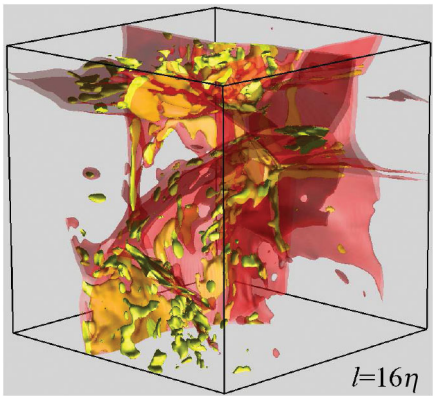

FIG. 3 (color). Isosurfaces for the solenoidal and compressive components of SGS kinetic energy flux Π_l in a 512^3 subdomain (the filter width $l = 16\eta$). (1) Yellow surfaces for $\Pi_l^s = 12.0(\Pi_l^s)^{\mathrm{rms}}$, and (2) red surfaces for $\Pi_l^c = 12.0(\Pi_l^c)^{\mathrm{rms}}$.

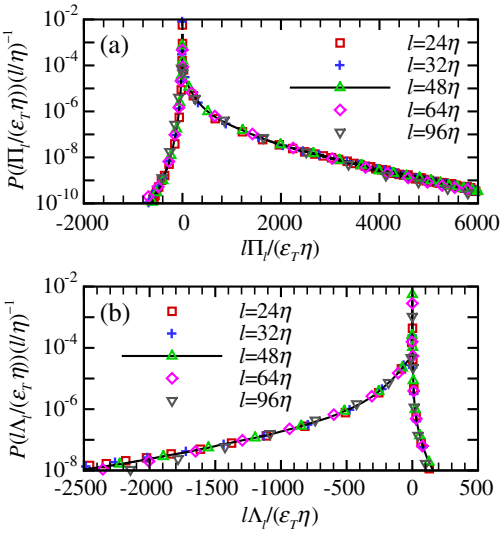

FIG. 4 (color online). Rescaled probability distribution functions (a) $P[l\Pi_l/(\epsilon_T\eta)](l/\eta)^{-1}$ and (b) $P[l\Lambda_l/(\epsilon_T\eta)](l/\eta)^{-1}$.

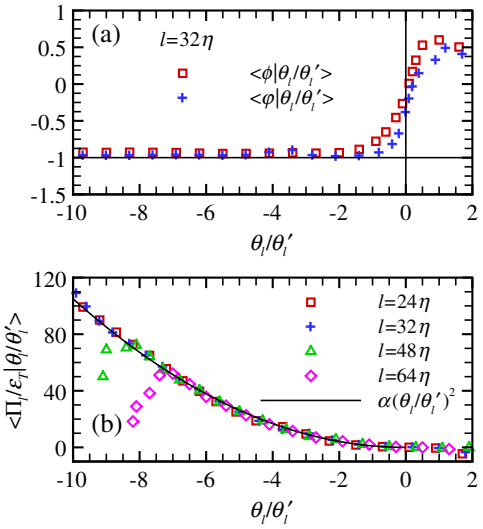

FIG. 5 (color online). (a) Conditional average of ψ and ϕ; (b) conditional average of Π_l.

energy flux component compared to its solenoidal counterpart.

The rescaled probability distribution functions (PDFs) of the SGS kinetic energy flux are depicted in Fig. 4. The rescaled PDFs of Π_l exhibit a strong skewness toward the positive side, showing a substantial difference from the case of incompressible turbulence [27], wherein the PDFs of the SGS energy flux have a moderate skewness. Therefore, most of the kinetic energy transfer due to the SGS stress is from large scales to small scales. Meanwhile, the rescaled PDFs of Λ_l display a strong skewness toward the negative side, indicating that most of the kinetic energy transfer due to the SGS mass flux is from small scales to large scales. We note that the extended and long PDF tails of the SGS kinetic energy flux have a major contribution from shock regions. Moreover, the tails of the rescaled PDFs of the SGS kinetic energy flux collapse to the same distribution for all l in the inertial range. According to the multifractal theory [26], the scaling exponents for the moments of $l\Pi_l$ and $l\Lambda_l$ should saturate at the value of $z_\infty = 1$ for high orders, namely, $\langle|l\Pi_l|^n\rangle \sim l^{z_\infty}$ and $\langle|l\Lambda_l|^n\rangle \sim l^{z_\infty}$ for large n. This prediction reveals a statistical scale-invariant property of energy flux in the inertial range and demonstrates the similarity between compressible turbulence and 1D Burgers turbulence [28].

To further clarify the impact of shock waves on kinetic energy transfer, we apply the average of various quanties conditioned on the filtered dilatation $\theta_l = \nabla\cdot\tilde{\mathbf{u}}$. Figure 5(a) depicts the conditional average of ψ and ϕ for $l=32\eta$, where $\psi = \tilde{\mathbf{S}}:\tilde{\tau}/(|\tilde{\mathbf{S}}||\tilde{\tau}|)$ and $\phi = \nabla\bar{p}\cdot(\overline{\rho\mathbf{u}} - \bar{\rho}\,\tilde{\mathbf{u}})/(|\nabla\bar{p}||(\overline{\rho\mathbf{u}} - \bar{\rho}\,\tilde{\mathbf{u}})|)$. Here, the large-scale strain is $\tilde{\mathbf{S}} = (\nabla\tilde{\mathbf{u}} + \nabla\tilde{\mathbf{u}}^T)/2$ and the SGS stress is $\tilde{\tau} = [\bar{\rho}(\widetilde{\mathbf{u}\mathbf{u}} - \tilde{\mathbf{u}}\,\tilde{\mathbf{u}})]$. Both the averages ψ and ϕ are close to -1 for $\theta_l/\theta_l' < -2$, indicating antiparallel alignments between the large-scale strain and the SGS stress, and between the pressure gradient and the turbulent mass flux vector in shock regions. The perfect alignments maximize the SGS kinetic energy flux, which is a distinctive feature of shock structures in comparison to vortex structures. In 3D incompressible turbulence, vortex dynamics induces a considerably weaker alignment between the large-scale strain and the SGS stress. For strong positive filtered dilatation, there is a tendency of parallel alignment between the large-scale strain and the SGS stress, indicating that an inverse cascade of kinetic energy due to SGS stress occurs locally in strong expansion regions. We plot the average of the SGS kinetic energy flux conditioned on the normalized filtered dilatation in Fig. 5. The conditional average of normalized Π_l is well approximated by $\alpha(\theta_l/\theta_l')^2$ in compression regions, where $\alpha = 1.05$ for filter widths l in the inertial range. This observation is consistent with the kinetic energy cascade scenario [10–12], as well as the fact that the local viscous dissipation of kinetic energy increases linearly with the square of dilatation in shock regions [21].

Finally, we emphasize that the $k^{-5/3}$ spectrum of the overall kinetic energy and the k^{-2} spectrum of the compressive kinetic energy are revealed at a moderate turbulent Mach number. As Mach number increases, the interactions between the solenoidal and compressive modes will become stronger, probably leading to a tendency of energy equipartition between the two modes [29]. Previous studies on numerical simulations of Euler equations showed that the spectrum exponents for both the solenoidal and compressive velocity are very close to -2 at high Mach numbers [8,16]. However, the simulations might be substantially contaminated by the excessive numerical dissipation of low-order schemes in these works. Therefore, several issues require further investigations through high-order numerical simulations, including the spectrum of solenoidal velocity and the effect of density variations on the kinetic energy spectrum at high turbulent Mach numbers.

The authors appreciate the valuable discussions with professor L.-P. Wang. This work was supported by the National Natural Science Foundation of China (Grants No. 11221061 and No. 91130001) and the National Science and Technology Ministry under a subproject of the 973 Program (Grant No. 2009CB724101). The simulations were done on the TH-1A super computer at Tianjin, China. Y. Y. is also supported partially by NSFC Grant No. 11274026 and China Postdoctoral Foundation Grant No. 2011M500194.

*ypshi@coe.pku.edu.cn
†syc@pku.edu.cn

[1] P. Sagaut and C. Cambon, *Homogeneous Turbulence Dynamics* (Cambridge University Press, Cambridge, England, 2008).
[2] P. Padoan and A. Norlund, Astrophys. J. **576**, 870 (2002).
[3] U. Frisch, *Turbulence: The Legacy of A. N. Kolmogorov* (Cambridge University Press, Cambridge, England, 1995).
[4] J. Cardy, G. Falkovich, and K. Gawedzki, *Non-equilibrium Statistical Mechanics and Turbulence* (Cambridge University Press, Cambridge, England, 2008).
[5] J. W. Armstrong, B. J. Rickett, and S. R. Spangler, Astrophys. J. **443**, 209 (1995).
[6] N. Kevlahan and R. Pudritz, Astrophys. J. **702**, 39 (2009).
[7] H. Xu, H. Li, D. C. Collins, S. Li, and M. L. Norman, Astrophys. J. **725**, 2152 (2010).
[8] A. G. Kritsuk, M. L. Norman, P. Padoan, and R. Wagner, Astrophys. J. **665**, 416 (2007).
[9] W. Schmidt, C. Federrath, and R. Klessen, Phys. Rev. Lett. **101**, 194505 (2008).
[10] H. Aluie, Phys. Rev. Lett. **106**, 174502 (2011).
[11] H. Aluie, Physica (Amsterdam) **247**, 54 (2013).
[12] H. Aluie, S. Li, and H. Li, Astrophys. J. Lett. **751**, L29 (2012).
[13] J. Wang, L.-P. Wang, Z. Xiao, Y. Shi, and S. Chen, J. Comput. Phys. **229**, 5257 (2010).
[14] S. Kida and S. A. Orszag, J. Sci. Comput. **5**, 85 (1990).
[15] M. R. Petersen and D. Livescu, Phys. Fluids **22**, 116101 (2010).
[16] C. Federrath, J. Roman-Duval, R. S. Klessen, W. Schmidt, and M.-M. Mac Low, Astron. Astrophys. **512**, A81 (2010).
[17] See Supplemental Material at http://link.aps.org/supplemental/10.1103/PhysRevLett.110.214505 for a brief description of large versions of Figs. 1(a) and 2(c) and also contains derivations of the governing equations for the velocity potential and physical-space flux relation.
[18] J. Bec and K. Khanin, Phys. Rep. **447**, 1 (2007).
[19] H. Miura and S. Kida, Phys. Fluids **7**, 1732 (1995).
[20] B. Thornber and Y. Zhou, Phys. Rev. E **86**, 056302 (2012).
[21] R. Samtaney, D. I. Pullin, and B. Kosovic, Phys. Fluids **13**, 1415 (2001).
[22] G. Falkovich, I. Fouxon, and Y. Oz, J. Fluid Mech. **644**, 465 (2010).
[23] S. Galtier and S. Banerjee, Phys. Rev. Lett. **107**, 134501 (2011).
[24] R. Wagner, G. Falkovich, A. G. Kritsuk, and M. L. Norman, J. Fluid Mech. **713**, 482 (2012).
[25] N. Cao, S. Chen, and Z. S. She, Phys. Rev. Lett. **76**, 3711 (1996).
[26] R. Benzi, L. Biferale, R. T. Fisher, L. P. Kadanoff, D. Q. Lamb, and F. Toschi, Phys. Rev. Lett. **100**, 234503 (2008).
[27] Q. Chen, S. Chen, G. L. Eyink, and D. D. Holm, Phys. Rev. Lett. **90**, 214503 (2003).
[28] J. Wang, Y. Shi, L.-P. Wang, Z. Xiao, X. T. He, and S. Chen, Phys. Rev. Lett. **108**, 214505 (2012).
[29] R. H. Kraichnan, J. Acoust. Soc. Am., **27**, 438 (1955).